Check for updates

Controlled release of carnosine from poly(lactic-*co*-glycolic acid) beads using nanomechanical magnetic trigger towards the treatment of glioblastoma†

Kinana Habra, [a] Robert H. Morris, [a] Stéphanie E. B. McArdle [b] and Gareth W. V. Cave [*a]

Nanometer scale rods of superparamagnetic iron oxide have been encapsulated, along with the anti-cancer therapeutic carnosine, inside porous poly(lactic-*co*-glycolic acid) microbeads with a uniform morphology, synthesised using microfluidic arrays. The sustained and externally triggered controlled release from these vehicles was demonstrated using a rotating Halbach magnet array, quantified *via* liquid chromatography, and imaged *in situ* using magnetic resonance imaging (MRI) and scanning electron microscopy (SEM). In the absence of the external magnetic trigger, the carnosine was found to be released from the polymer in a linear profile; however, over 50% of the drug could be released within 30 minutes of exposure to the rotating magnetic field. In addition, the release of carnosine embedded on the surface of the nano-rods was delayed if it was mixed with the iron oxide nano rods before the encapsulation. These new drug delivery vesicles have the potential to pave the way towards the safe and triggered release of onsite drug delivery, as part of a theragnostic treatment for glioblastoma.

Glioblastoma multiforme (GBM) is the most aggressive form of brain cancer with patients generally dying within 15 months after diagnosis.[1,2] The complete removal of brain tumours cannot be achieved by surgery alone due to the complex finger-like structure of the tumour cells and their migration away from the bulk of the tumour.[3] In addition, these tumours are highly resistant to current radiation and chemotherapy treatments.[4,5] Therefore, there is an urgent need to look towards new therapeutic strategies to treat this fatal disease.[6] We have previously demonstrated that carnosine can be safely utilised as a potential therapy in this area, however, the model of delivery and release of the active substrate requires further investigation.[7] One of the most promising options for this release is the application of a time varying external magnetic field.

Magnetic fields have found application in many clinical applications since they are not inherently damaging to the body, though therapies often lack selectivity and locality.[8] Current research strategies therefore often couple the application of magnetic fields with biochemical and physical properties of some additional agent to aid in overcoming these limitations.[9–14] Specifically, the adoption of nanometre scale paramagnetic materials into such therapies enhanced the localisation effect, while also reduced the biotoxicity.[15,16] The biomedical application of functionalised paramagnetic nanoparticles has stimulated much interest, specifically in nano-magneto mechanical activation (NMMA) by non-heating low-frequency alternating magnetic fields ($f < 1$ kHz). The nanoparticles act as mediators that localise and apply forces to target biomolecular structures including enzymes, transport vesicles and cell organelles, without significant heating. Therefore, NMMA demonstrates a biophysical platform for various therapies including the sustained and controlled release of therapeutics, without increasing toxicity.[17] Paramagnetic nanoparticles have been used as non-thermal contrast reagents in magnetic resonance imaging and as carriers in drug delivery by nanoscale modules.[18,19] However, clusters of superparamagnetic nanoparticles have also been demonstrated to induce magnetic hyperthermia therapies when enshrouded with a polymer coating, impregnated with a drug.[20,21] Therefore, introducing paramagnetic nanoparticles to a living organism can result in both thermal and non-thermal therapies; simply by changing the frequency of the alternating magnetic field.[17] These combined properties have successfully been utilised to induce controlled drug release from a nanoscale vector.[22,23]

In oncology, NMMA techniques have been employed for the deformation of molecular structures, where in, the paramagnetic nanoparticles are utilised to manipulate the sensitivity of tissue, cells, and vesicles.[17,24] The biochemical response to this mechano-transduction is cell death, or apoptosis,.[24–26] It

aSchool of Science and Technology, Nottingham Trent University, Nottingham NG11 8NS, UK. E-mail: kinana.habra2017@ntu.ac.uk; rob.morris@ntu.ac.uk; gareth.cave@ntu.ac.uk; Tel: +44(0)-115-848-3242

bJohn van Geest Cancer Research Centre, School of Science and Technology, Nottingham Trent University, Nottingham NG11 8NS, UK. E-mail: stephanie.mcardle@ntu.ac.uk

† Electronic supplementary information (ESI) available. See DOI: 10.1039/d2na00032f

has, unfortunately, also been seen to stimulate tumour growth. This is attributed to the transmission of force from the rigid malignant cells to the soft surrounding healthy ones, leading to metastasis.[27] Functionalising the paramagnetic nanoparticles and utilising magnetic actuation to trigger mechanical forces offers an exciting strategy to remotely control the drug release from coupled magnetic materials.[28] The contactless mechanical disruption of the polymer coating triggers the release of the therapeutic material which triggers apoptosis cascade within the targeted cells.[27] This physical stimulation has been showed to be advantageous, compared to photon or thermal triggering, thanks to the possibility of achieving deep activation in a controllable and non-invasive manner for *in vivo* applications.[29]

Recently, we reported the method of formulating carnosine with superparamagnetic nano-rods of magnetite (Fe_3O_4) towards the controlled release treatment at the targeted GBM cells by applying mild hyperthermia.[7] To improve the preliminary model, the conjugated nanorods and carnosine from our previous work were embedded in microbeads of poly(lactic-*co*-glycolic acid) (PLGA) as a potential magnetically triggered drug delivery device. PLGA is commonly used in the synthesis of clinical drug delivery systems, specifically for drug molecules with short half-life protein structures, as the PLGA constructs have been showed to increase the bioavailability of the drugs.[30–32] Traditional methods for making PLGA emulsions involve manual or mechanical agitation. However, such stresses are conducive to control uniformity across the system.[33] Controlling both the structure and function of polymeric drug delivery has been optimised using microfluidic method, *via* the flow-directed shear processing in a two-phase microfluidic reactor.[34] In general, such microfluid techniques have been accepted as applicate scale-up strategies, namely, Factory-on-Chip techniques which achieved high throughput synthesis to enhance the industrial production scale.[35] Synthetic size-tuneable PLGA microparticles have now been effectively produced by combining modern technologies of artificial intelligence and microfluidics, thereby improving efficiency and performance.[36]

Herein, we describe a microfluidic double emulsification method that encapsulates and retains the dipeptide carnosine and Iron Oxide Nano Rods (IONRs) within the polymeric microcapsules. The synthesis, characterisation, and stability profile for the IONRs (*ca.* 85 nm) have been described in our previous work (Fig. S1†).[7] The encapsulate is a spherical protective wall material (bead) consisting of empty chambers in a stable emulsion. These sequential emulsifications enable highly efficient encapsulation with precisely tuneable beads size (*ca.* 10 μm) with rigid shells. The mechanical trigger embeds the carnosine into the surface of the IONRs if they were in the same space and only a mild hyperthermia trigger is needed for the release. However, if the carnosine and IONRs were in different beads, the mechanically induced spinning of the IONRs releases the carnosine from the beads instead of attaching it. This methodology can be further extended to encapsulate multiple drugs and manipulate the release depending on the application requirement. The aim therefore is to use the paramagnetic magnetic nanoparticles as a controlled trigger for the release and medical imaging. Thereby avoiding the need to subject the patient to multiple therapeutic injections and enable the physician to trigger the non-invasive delivery of carnosine at the optimised time and dose. This drug delivery methodology has the potential to be described as an on-demand wireless personalised smart drug delivery system, that can be conducted inside a conventional MRI scanner.

Utilising carnosine within a sustained release designed experiment resulted in the inhibition of single spheroid growth compared to the untreated spheroid. This experiment reflects the importance of the sustained release of carnosine for the treatment of the brain tumour. The change in single spheroids' morphology was monitored using the IncuCyte spheroids software over 5 days. The first 24 hours were used to grow the single spheroid, followed by the carnosine treatment which was added every 48 hours starting from 0 hour (Fig. S2†). The product application is a non-invasive strategy of convection enhanced delivery by direct injection and implementation inside the brain tumour tissues or after the surgery of tumour removal. The beads are not prepared for another route application such as intravenous. After applying a colloid of the beads with the media of the cell line, the beads showed attachment to the outer surface membrane of the monolayer cells due to the negative zeta potential. The transmembrane transport was affected by the micro size of the beads, in that it was reduced as a result of the steric hindrance of the localisation of the beads on the membrane, however, both passive or active movement of the beads once localised is insignificant.[37] Moreover, cell membranes have an electrical potential across them (negative intracellular), leading to a membrane potential that facilitates positively charged substrates to flow into the cell.[38] Thus, the beads became stuck to the outer surface, and it was not possible to remove them by washing with media or PBS after 24 hours. Bioerodible implants made up of polymeric materials have been discussed in the literature of over five decades.[39] The ability to disperse drug molecules throughout thermally stable biodegradable polymers such as PLGA, results in active polymer matrix which enabled a degree of control over this release profile while the polymers are metabolised by the body.[40,41] However, clinical PLGA formulations are not yet widespread due to their low drug loading of hydrophilic small molecules, high initial burst release, and poor stability. Low-temperature double-emulsion strategies,[42] enables the synthesis of clinically viable *in situ* swellable (carnosine or IONRs) loaded PLGA beads. The beads production was repeatedly and consistently performed using microfluidic hydrodynamic flow focusing systems enabling multiple emulsifications.[43] The adoption of a micromixer chips to such a device enabled the hydrophobic materials to be encapsulated inside shells of PLGA, then packaged by the second emulsification into PLGA microbeads.

Empty beads of PLGA were prepared by using a Dolomite microfluidic flow focus system.[43] Continuous microscopic observation was applied during the double emulsification to monitor the mixing of the water and PLGA phases inside the chip. Microscopic images were taken for the PLGA beads on glass slide directly after the double emulsification. The larger

PLGA beads (>100 μm) were observed to shrink after around 5 minutes in air, drying to less than 100 μm, with complete solvent evaporation occurring after an additional 5 minutes achieving a final size of the PLGA around 10 μm, as seen in Fig. 1. The system was found the have an encapsulation efficiency, EE% > 99%, and loading efficiency, LE% = 33.4%.

FT-IR spectroscopy of the IONRs, L-carnosine and PLGA empty beads (PLGA and PVA), resulted in characteristic IR vibrational peaks in the high-frequency region were the stretching vibration at 2162 cm^{-1} and 1643 cm^{-1} is due to
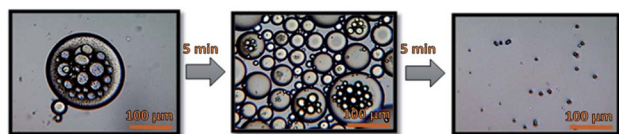
vibrational bending of carnosine imidazole (N–H),[44] stretching at 800 cm^{-1} from the IONR and the alkane (C–H) at 2200 cm^{-1},[45] and a strong absorption peak at 1738 cm^{-1} from the carbonyl (C=O) group stretching for the loaded polymer beads.[46] These results provided evidence that the carnosine and IONRs were encapsulated with the PLGA, with the characteristic bands overlapped in the spectrum of the new drug delivery device (Fig. S3†). Fig. 2 shows the blank beads of 0.1% PLGA with sponge like shape. Increasing the concentration of the PLGA to 1% showed a morphology of tight PLGA beads with less holes on the walls. Rhodamine-B was used in 1% concentration to trace the aqueous phase which will facilitate later indication of carnosine during the carnosine encapsulation. A uniformity in water phase distribution was observed with the confocal images where the red seeds of water with similar size were evenly spread inside the PLGA beads. The microfluidic double emulsification using the microfluidic system was shown to be a highly reproducible method to synthesis uniform PLGA beads which ensure the uniformity of dosage form per sample.[36]
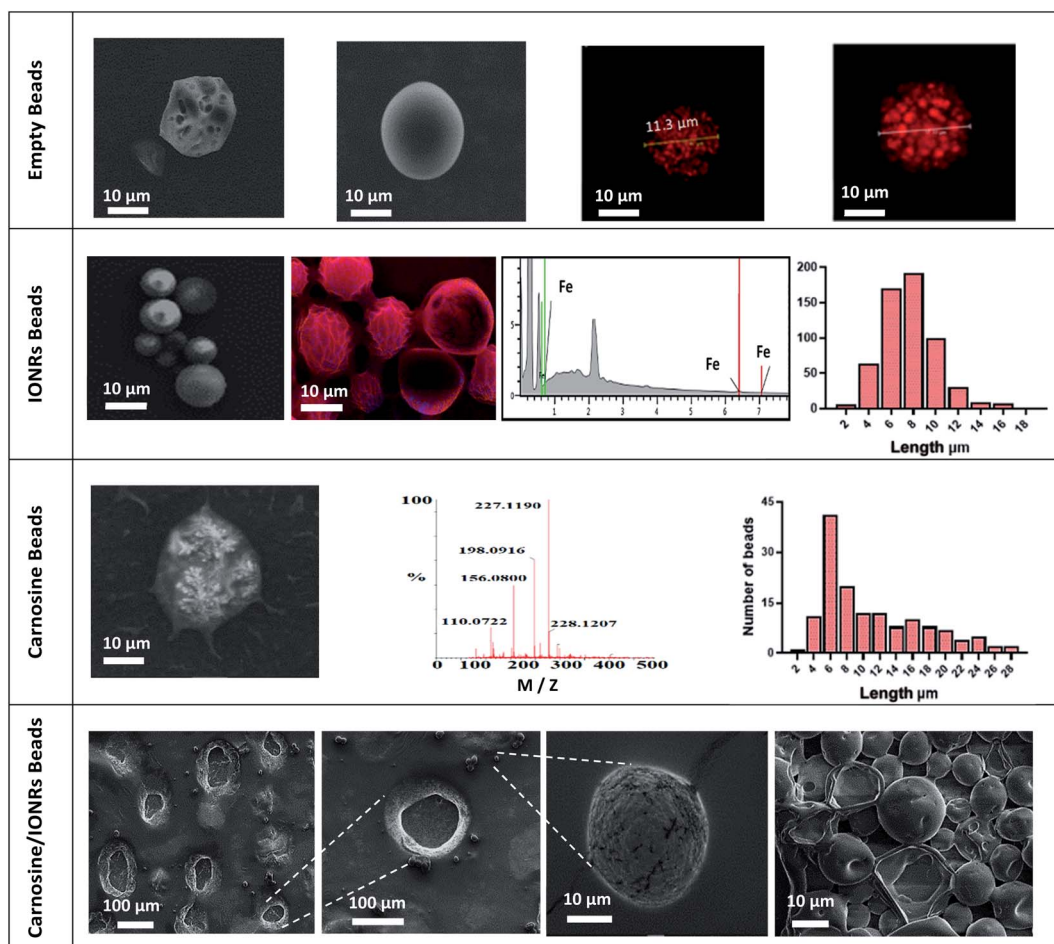

Fig. 1 Microscopic images for PLGA beads after encapsulation and during evaporation.

Fig. 2 Empty beads, SEM images compare between the characterisation of empty (0.1%, 1% PLGA beads) and the uniform distribution of the water phase inside the beads. IONRs beads, SEM images for IONRs loaded 0.1% PLGA beads, EDS mapping the blue colour of iron traces inside the red carbon colour of the PLGA, and the iron peaks confirm the images. The histogram refers to a mean diameter size of 7.4 ± 2.3 μm. Carnosine beads, SEM images for carnosine loaded 1% PLGA beads, MS spectrum identifies the peaks of carnosine pattern. The histogram refers to a mean diameter size of 11.6 ± 7.0 μm. Carnosine/IONRs beads, SEM images for (carnosine & IONRs) loaded 1% PLGA beads. The size of the beads/shells shifts to be 10 times larger than the previous beads. All were open with fragile structure and most of the 10 μm shells were destroyed.

Following the hydrothermal synthesis to produce IONRs of 86 ± 17 nm length,[7] the nanorods were encapsulated to obtain 0.1% PLGA microbeads. The mean final diameter of the dry IONR beads was 7.4 ± 2.3 μm. The same method was applied to produce the carnosine beads. However, the LC-MS detection showed that carnosine leached from the beads. Thus, the concentration of PLGA was changed to 1% with carnosine. The size of carnosine loaded beads was 11.6 ± 7.0 μm. SEM/EDS for (carnosine & IONRs) loaded 1% PLGA beads proved the size shift of the beads and shells to be 10 times larger than the previous beads. All beads were open with fragile structures and most of the shells were destroyed (Fig. 2).

It is well established that the interstitial pressure, stiffness and hyperproliferative pressure of fibrotic tumours can lead to enhanced tumour growth development.[27] Previously, mitochondria-targeted iron oxide nanoparticles were designed as nano-spinners to exert mechanical forces, under a rotating magnetic field, towards the treatment of cancers.[26]

Recently, it was proven that iron oxide nano-rods of around 70 nm are not localised in the mitochondria which make them safer as drug carriers. However, the same nano-rods moved from the stiff tumour tissue to the soft healthy surrounding cells upon spinning them remotely by an external rotating magnetic field (Fig. 3). A concentrated nano-rod suspension was placed in a premade hole inside a 2% agarose gel to mimic the movement of the nano-rods over time as a result of an externally applied rotating magnetic field, applied in this case using a rotating Halbach array (NdFeB N45, Bunting, Berkhamsted UK). ImageJ was used to apply a threshold to the image showing only the dark areas representing the nano-rods.[47] This showed a 2% increase, with an expansion of the perimeter of 25% after the application of the rotating magnetic field. Thus, the nano-rods did not cluster or aggregate though they did cause disruption to the gel in which they were placed (Fig. 3).

An *ex vivo* study using 6 brains of sacrificed male mice showed that encapsulating the iron oxide nano-rods inside PLGA microbeads ceased the spreading of the IONRs. After positioning the brain (2 mm lateral to the sagittal suture and 2 mm posterior to the coronal suture) 5 μL of IONRs suspensions (free/encapsulated) were injected 3 mm deep using a neuro-syringe, then were compared with empty PLGA beads.

The empty beads had no effect on the signal intensity of the MRI images, whilst the IONRs of 25 ppm and 50 ppm concentration showed a decrease in signal intensity. In comparison, the IONR beads of same concentration showed less contrast. A further MRI analysis was undertaken simultaneously to evaluate this process by determining the effective spin lattice relaxation time constant (T_2^{eff}) since the paramagnetic properties of the nano-rods are known to shorten this value.[48] The coronal images were collected using the MRI system with multi echo imaging sequence. The echo time was 7.8 ms and 32 echo images were collected with a repetition time of 5000 ms. MATLAB (Mathworks, MA) was used to undertake pixelwise fitting of a mono-exponentially function to the images to produce a T_2^{eff} map. The control empty beads T_2^{eff} (601 ms) was higher than the free IONRs T_2^{eff} (336 ms) (Fig. 4). There is an observed decrease in the spin echo when the IONRs were inside the beads. However, the difference is not expected to be significant because the system is designed to enable free rotation of the IONR, resulting in both the shear and the contrast effects which will increase when they release from the beads.

For carnosine investigations, the sustained release simulation from PLGA beads was studied by performing a dialysis membrane experiment. The mechanical rotation was created by a magnetic stirrer bar rotating inside the membrane bag with controlled speeds. The comparison was between 100 rpm which simulates the human fluid dynamics and 1000 rpm which demonstrates the potential shear stress from the rotation of the IONRs.[49] The rotation of the IONRs produces both centrifugal and shear stresses forces, much in the same way as the paddles of the described dissolution apparatus in the British Pharmacopoeia, dissolution testing monographs. Over a week of mechanical stirring, the SEM images showed the beads developing holes into the inner chambers which allowed the
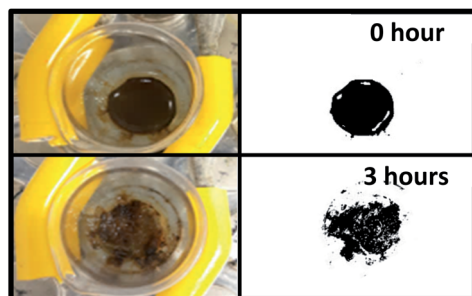

Fig. 3 The effect of a rotating Halbach array on a suspension of nano-rods embedded in agarose (2% w/v) over time. Masking the dark areas showed the difference before and after 3 hours of external magnetic rotation.
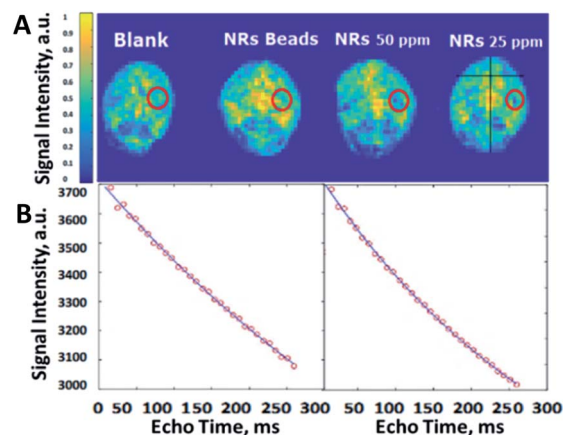

Fig. 4 (A) *Ex vivo* MRI images of the mice brains injected with IONRs. The location of injected beads of IONRs or controls is shown by red circles. The colour codes the signal intensity which is proportional to the value of T_2^{eff} in ms. The signal is shown to decrease in intensity for the 50 ppm and 25 ppm areas confirming the presence of a negative contrast agent which is expected from the IONPs. (B) Comparative curves of the control (left) and IONRs beads (right) showed the drop in signal intensity as a function of echo time, with a steeper change in the case of free IONRs indicating a shorter T_2^{eff}.

carnosine to be released gradually. The samples were retained for a month, then the beads were imaged empty (Fig. 5A). The IONRs were well tolerated by the U87 malignant and differentiated cells, and the tracking of the intracellular uptake showed their safety and biodegradability.[7] All beads were purified using bacterial filtration (sintered funnel grade 5; porosity 1 to 1.6 μM) and sterilised with 70% ethanol. Swabs of each bead formulation were applied to a tryptic soy agar (TSA) plate. The plates were incubated at 35 °C for five days. No bacterial or fungal colony growth were observed.

The final component for the beads was either PLGA loaded with carnosine and the LC-MS was used for the assay, or PLGA loaded with iron oxide nanorods which was measured by the ICP-MS. The daily monitoring for the carnosine release by LC-MS showed that 50% of the total carnosine was released after 24 hours. Afterwards, 10% of carnosine was released daily over a week (Fig. 5B). The cumulative release of carnosine increased 20% as a result of the mechanical forces applied by the rotating magnetic field. Dynamic light scattering (DLS) measurements supported the change in the beads' diameters (Fig. S4†).

Finally, to investigate the potential application of rotating magnetic fields for cancer treatment, we designed a combination formulation using carnosine loaded with IONRs to optimise a controlled delivery and targeted treatment. A schematic of the rotating magnetic system can be found in Fig. 6A and S5†
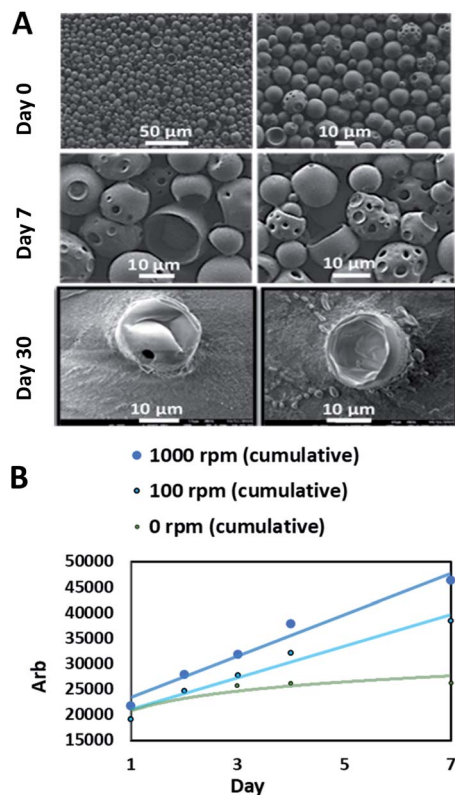

Fig. 5 Membrane dialysis experiment. (A) SEM images show the PLGA beads in the beginning which had holes in the structure after a week and became completely empty after a month. (B) The LC-MS cumulative analysis for the released carnosine shows faster release from the beads which were exposed to the higher mechanical rotation.
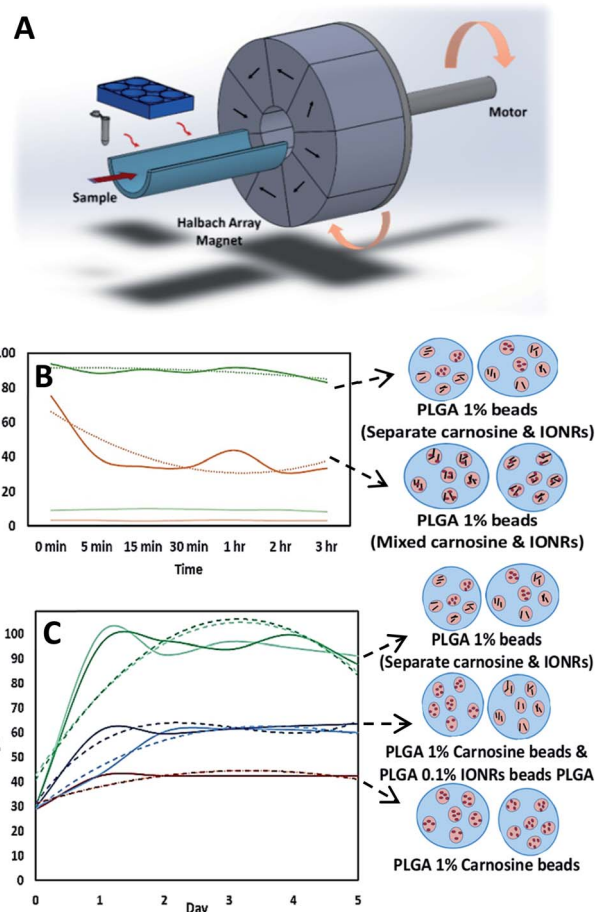

Fig. 6 (A) Schematic illustration for the rotating magnet system designed for this application. The arrows indicate the direction of the magnetic field which produce an intense uniform magnetic field within their central air gap, and zero field outside. (B) LC-MS assay for the normalised concentrations of carnosine show the advantage of using the hydrophobic chip (dark curves) the hydrophilic chip (light curves) for the initial emulsification. (C) LC-MS assay for the normalised concentrations of carnosine show the comparison between adding the encapsulated IONRs to the carnosine before or after the initial emulsification. Curves with light colours are for beads before the application of magnetic field and the curves with dark colours are for after the application of magnetic field. Red spheres are carnosine and black rods are IONRs. The dotted lines are trend lines fitted to the normalised concentration of the released carnosine.

supported the magneto mechanical non-heating effect for a 1 Tesla rotating magnetic field during the first 30 minutes at 20 Hz.[19] To enhance the potential clinical uptake of this anti-cancer medical drug delivery device, PLGA-based carrier and Fe_3O_4 SPIOS were targeted as a pre-approved FDA reagent for therapeutic applications.[50] Micro-scale beads are predicted to circulate *in vivo* without aggregation while the submicron size of nanoparticles enable enhanced intracellular uptake.[51] The carnosine was observed to leach out of the beads due to its inherent smaller sizes and flexibility. A concentration of 1% PLGA was sufficient to retain the embedded carnosine and be released *via* the rotation of IONRs from the beads, while at 0.1% PLGA the dug was lost to the media without any stimuli.

The preparation of the beads was reproducible under the same parameters of flow rate and pump pressure at room temperature. The drug release experiment using the magnetic field as a trigger, showed the trend of the release and monitoring the release by the IONRs imaging, is key for personalising the release in response the tumour recurrence, incuding location, size, and resistance.

Although the flow speed dominates, directing the liquids towards creating a central stream for the inner phase, changing the hydrophobicity of the micromixer chip to match the outer phase of the emulsion was critical in each step (Fig. 6B). The drug entrapped in a PLGA matrix was released at a sustained rate because of the degradation of the polymer which can be varied according to the block copolymer molecular weight and composition.[52] Each type of nano-shell (IONRs and carnosine) could be packaged in PLGA beads separately or as a mixture, before the second emulsification. Mixing the IONRs with the carnosine before the initial emulsion showed a reduction in the detection of carnosine over 3 hours (Fig. 6B). The carnosine was attached over time on the surface coating of the IONRs and retained until triggered by mild hyperthermia as we previously demonstrated.[7] However, mixing the separate shells of carnosine and IONRs produced unstable beads, and both leaked out during the evaporation step. The ICP-MS assay supported the instantaneous release for the IONRs (Fig. S6†). The formulation of 1% PLGA carnosine beads and 0.1% PLGA IONRs beads found similar outcomes to the dialysis experiment by showing a surge in the total amount of carnosine when the nano IONRs were spun for 30 minutes. Having the IONRs in the same vicinity with the carnosine attracted the carnosine out of the beads because of electric surface charge forces. However, applying the non-heating 30 rotating magnetic field for 30 minutes increased the speed of carnosine release due to mechanical micro-deformation of the PLGA outer structure with the rotating nano particles (Fig. 6C). This degradation is an outside-in mechanical process, whereas *in vitro* inside-out degradation is thought to occur in PLGA microbeads as a result of the autocatalytic process.[53]

The comparison between the three previous formulations showed how changing any parameter may result in a critical change. However, these variables could always be utilised to produce different types of PLGA beads for controlled, delayed, or sustained release. Freeze drying the beads is crucial for long-term stability and storage conditions (4 °C/ambient humidity).[54-56] This keeps the product ready to be rehydrated with sterilised water at the time of use. However, measuring zeta potential showed that applying gentle vacuum drying reduced the fragility of the beads which resulted in carnosine being released as waves over 15 days instead of the single initial burst (Fig. S7†). The stability of the beads should be taken into consideration owing to the fact that buffers contain relatively high sodium ion concentrations that are known to disturb electrostatic repulsion effects. The inclusion of serum in the media is essential, as its associated proteins are predominantly negatively charged at physiological pH, and therefore sterically hinder any potential agglomeration (Fig. S8†).[57]

Conclusions

Previously, we have demonstrated that carnosine inhibits the proliferation of glioblastoma U87 cancer cells, thereby reducing the risk of metastasis.[7] Therefore, the drug delivery system presented in this communication offers the potential to be implanted into the post-surgical cavity and used as a complimentary treatment to improve the prognosis of this devastating disease. As such, we are currently working towards an *in vivo* mouse model to demonstrate the potential clinical viability of this work.

Data availability

The data presented in this study are available on request from the corresponding author.

Author contributions

K. H. performed the experiments and wrote the first draft. R. H. M performed the *ex vivo* MRI, constructed the magnetic rotation system and contributed to the final manuscript. G. W. V. C contributed to experimental design and final manuscript. All authors have read and agreed to the published version of the manuscript.

Conflicts of interest

The authors declare no conflict of interest.

Acknowledgements

References

1 Y. Jiang and L. Uhrbom, On the origin of glioma, *Upsala J. Med. Sci*, 2012, **117**, 113–121.

2 Q. T. Ostrom, H. Gittleman, G. Truitt, A. Boscia, C. Kruchko and J. S. Barnholtz-Sloan, CBTRUS Statistical Report: Primary Brain and Other Central Nervous System Tumors Diagnosed in the United States in 2011–2015, *Neuro-Oncology*, 2018, **20**, 1–86.

3 M. Lara-Velazquez, R. Al-Kharboosh, S. Jeanneret, C. Vazquez-Ramos, D. Mahato, D. Tavanaiepour, G. Rahmathulla and A. Quinones-Hinojosa, Advances in Brain Tumor Surgery for Glioblastoma in Adults, *Brain Sci.*, 2017, **7**, 166.

4 S. Bao, Q. Wu, R. McLendon, Y. Hao, Q. Shi, A. B. Hjelmeland, M. W. Dewhirst, D. D. Bigner and J. N. Rich, Glioma stem cells promote radioresistance by

preferential activation of the DNA damage response, *Nature*, 2006, **444**, 756–760.

5 K. Messaoudi, A. Clavreul and F. Lagarce;, Toward an effective strategy in glioblastoma treatment. Part I: resistance mechanisms and strategies to overcome resistance of glioblastoma to temozolomide, *Drug Discovery Today*, 2015, **20**, 899–905.

6 S. Cuzzubbo, S. Mangsbo, D. Nagarajan, K. Habra, A. G. Pockley and S. E. B. McArdle, Cancer Vaccines: Adjuvant Potency, Importance of Age, Lifestyle, and Treatments, *Front. Immunol*, 2021, 3850.

7 K. Habra, S. E. B. McArdle, R. H. Morris and G. W. V. Cave, Synthesis and Functionalisation of Superparamagnetic Nano-Rods towards the Treatment of Glioblastoma Brain Tumours, *Nanomater*, 2021, **11**, 2157.

8 *Oxford Handbook of Oncology Cassidy*, ed. J. D. Bissett, R. Spence, M. Payne and G. Morris-Stiff, Oxford University Press, Oxford, 4th edn, 2015.

9 R. Duncan, Nanomedicine (s) under the microscope, *ACS Publications*, 2011, **8**, 2101–2141.

10 S. Bamrungsap, Z. Zhao, T. Chen, L. Wang, C. Li, T. Fu and W. Tan, Nanotechnology in therapeutics: A focus on nanoparticles as a drug delivery system, *Nanomedicine*, 2012, **7**, 1253–1271.

11 X. Zhang, X. Xu and N. Bertrand, Interactions of nanomaterials and biological systems: Implications to personalized nanomedicine, *Adv. Drug Delivery Rev.*, 2012, **64**, 1363–1384.

12 A. Quarta, C. Piccirillo and G. Mandriota, Nanoheterostructures (NHS) and their applications in nanomedicine: focusing on in vivo studies, *Mater*, 2019, **12**, 139.

13 L. Racca and V. Cauda, Remotely Activated Nanoparticles for Anticancer Therapy, *Nano-Micro Lett*, 2021, **13**, 11.

14 A. Wicki, D. Witzigmann, V. Balasubramanian and J. Huwyler, Nanomedicine in Cancer Therapy: Challenges, Opportunities, and Clinical Applications, *J. Controlled Release*, 2015, **200**, 138–157.

15 O. Noqta, A. Aziz and I. Usman, Recent advances in iron oxide nanoparticles (IONPs): synthesis and surface modification for biomedical applications, *J. Supercond. Novel Magn.*, 2019, **32**, 779–795.

16 P. Majewski and B. Thierry, Functionalized Magnetite Nanoparticles—Synthesis, Properties, and Bio-Applications, *Crit. Rev. Solid State Mater. Sci.*, 2007, **32**, 203–215.

17 Y. I. Golovin, D. Y. Golovin, K. Y. Vlasova, M. M. Veselov, A. D. Usvaliev, A. V. Kabanov and N. L. Klyachko, Non-Heating Alternating Magnetic Field Nanomechanical Stimulation of Biomolecule Structures via Magnetic Nanoparticles as the Basis for Future Low-Toxic Biomedical Applications, *Nanomater*, 2021, **11**, 2255.

18 I. Armenia, M. Bonavia and L. Matteis, Enzyme Activation by Alternating Magnetic Field: Importance of the Bioconjugation Methodology, *J. Colloid Interface Sci.*, 2019, **537**, 615–628.

19 Y. Cheng, M. E. Muroski, D. C. Petit, R. Mansell, T. Vemulkar, R. A. Morshed, Y. Han, I. V. Balyasnikova,

C. M. Horbinski, X. Huang, L. Zhang, R. P. Cowburn and M. S. Lesniak, Rotating magnetic field induced oscillation of magnetic particles for in vivo mechanical destruction of malignant glioma, *J. Controlled Release*, 2016, **223**, 75–84.

20 X. Liu, Y. Zhang, Y. Wang, W. Zhu, G. Li and X. Ma, Comprehensive understanding of magnetic hyperthermia for improving antitumor therapeutic efficacy, *Theranostics*, 2020, **10**, 3793–3815.

21 C. Caizer, Optimization Study on Specific Loss Power in Superparamagnetic Hyperthermia with Magnetite Nanoparticles for High Efficiency in Alternative Cancer Therapy, *Nanomater*, 2020, **11**, 40.

22 A. Hervault and N. T. Thanh, Magnetic nanoparticle-based therapeutic agents for thermo-chemotherapy treatment of cancer, *Nanoscale*, 2014, **6**, 11553–11573.

23 K. Hayashi, M. Nakamura and H. Miki, Magnetically Responsive Smart Nanoparticles for Cancer Treatment with a Combination of Magnetic Hyperthermia and Remote-Control Drug Release, *Theranostics*, 2014, **4**, 834–844.

24 M. Hsieh and H. Nguyen, Molecular mechanism of apoptosis induced by mechanical forces, *Int. Rev. Cytol.*, 2005, **245**, 321–346.

25 R. K. Jain, J. D. Martin and T. Stylianopoulos, The role of mechanical forces in tumor growth and therapy, *Annu. Rev. Biomed. Eng.*, 2014, **16**, 321–346.

26 M. Chen, J. Wu, P. Ning, J. Wang, Z. Ma, L. Huang, G. R. Plaza, Y. Shen, C. Xu, Y. Han, M. S. Lesniak, Z. Liu, Y. Cheng, M. W. Chen, J. J. Wu, P. Ning, J. J. Wang, Z. Ma, L. Q. Huang, Y. J. Shen, C. Xu, Z. M. Liu, Y. Cheng, G. R. Plaza, Y. Han and M. S. Lesniak, Remote Control of Mechanical Forces via Mitochondrial-Targeted Magnetic Nanospinners for Efficient Cancer Treatment, *Small*, 2019, **16**, 1905424.

27 F. Broders-Bondon, T. H. Nguyen Ho-Bouldoires, M. Fernandez-Sanchez and E. Farge, Mechanotransduction in tumor progression: The dark side of the force, *J. Cell Biol.*, 2018, **217**, 1571–1587.

28 D. E. H. Diab, P. Clerc, N. Serhan, D. Fourmy and V. Gigoux, Combined Treatments of Magnetic Intra-Lysosomal Hyperthermia with Doxorubicin Promotes Synergistic Anti-Tumoral Activity, *Nanomater*, 2018, **8**, 468.

29 Y. Svenskaya, B. Parakhonskiy, A. Haase, V. Atkin, E. Lukyanets, D. Gorin and R. Antolini, Anticancer drug delivery system based on calcium carbonate particles loaded with a photosensitizer, *Biophys. Chem.*, 2013, **182**, 11–15.

30 L. Brannon-Peppas, Recent advances on the use of biodegradable microparticles and nanoparticles in controlled drug delivery, *Int. J. Pharm.*, 1995, **116**, 1–9.

31 S. A. Hagan, A. G. A. Coombes, M. C. Garnett, S. E. Dunn, M. C. Davies, L. Illum, S. S. Davis, S. E. Harding, S. Purkiss and P. R. Gellert, Polylactide–Poly (ethylene glycol) Copolymers as Drug Delivery Systems. 1. Characterization of Water Dispersible Micelle-Forming Systems, *Langmuir*, 1996, **12**, 2153–2161.

32 Y. Budama-Kilinc, R. Cakir-koc, S. Kecel-gunduz, Y. Kokcu, B. Bicak, H. Mutlu and A. E. Oze, Novel NAC-loaded poly

(lactide-co- glycolide acid) nanoparticles for cataract treatment: preparation, characterization, evaluation of structure, cytotoxicity, and molecular docking studies, *PeerJ*, 2018, e4270.

33 R. Shah, H. Shum, A. Rowat and D. Lee, Designer emulsions using microfluidics, *Materials Today*, 2008, **11**, 18–27.

34 A. Bains, Y. Cao and S. Kly, controlling structure and function of polymeric drug delivery nanoparticles using microfluidics, *Mol. Pharmaceutics*, 2017, **14**, 2595–2606.

35 T. Han, L. Zhang, H. Xu and J. Xuan, Factory-on-chip: Modularised microfluidic reactors for continuous mass production of functional materials, *Chem. Eng. J.*, 2017, **326**, 765–773.

36 S. A. Damiati, D. Rossi, H. N. Joensson and S. Damiati, Designer emulsions using microfluidics, *Sci. Rep.*, 2020, **10**, 1–11.

37 J. Kulbacka, A. Choromańska, J. Rossowska, J. Weżgowiec, J. Saczko and M. P. Rols, Cell Membrane Transport Mechanisms: Ion Channels and Electrical Properties of Cell Membranes, *Adv. Anat., Embryol. Cell Biol.*, 2017, **227**, 39–58.

38 A. A. Ramahi and R. L. Ruff, Membrane Potential, *Encyclopedia of the Neurological Sciences*, 2014, pp. 1034–1035.

39 S. Yolles, Biodegradable polymeric article for dispensing drugs, *US Pat.*, US3887699A, 1975.

40 J. C. Johnson. *Sustained Release Medications*, New Jersey, 1st edn, 1980.

41 R. C. Mundargi, V. R. Babu, V. Rangaswamy, P. Patel and T. M. Aminabhavi, *J. Controlled Release*, 2008, **125**, 193–209.

42 F. Y. Han, K. J. Thurecht, A. K. Whittaker and M. T. Smith, Bioerodable PLGA-Based Microparticles for Producing Sustained-Release Drug Formulations and Strategies for Improving Drug Loading, *Front. Pharmacol.*, 2016, 185.

43 Inside Dolomite Labs, *PLGA Multiple Emulsions for Hydrophilic Drug Delivery*, Dolomite Microfluidics, https://www.dolomite-microfluidics.com/news/inside-dolomite-labs-plga-multiple-emulsions-for-hydrophilic-drug-delivery/, accessed October 10, 2021.

44 M. L. Branham, P. Singh, K. Bisetty, M. Sabela and T. Govender, Preparation, Spectrochemical, and Computational Analysis of L-Carnosine (2-[(3-Aminopropanoyl) amino]-3-(1H-imidazole-5-yl) propanoic Acid) and Its Ruthenium (II) Coordination Complexes in Aqueous Solution, *Mol*, 2011, **16**, 10269–10291.

45 J. Mohapatra, A. Mitra, H. Tyagi, D. Bahadur and M. Aslam, Iron oxide nanorods as high-performance magnetic resonance imaging contrast agents, *Nanoscale*, 2015, **7**, 9174–9184.

46 N. Schleich, P. Sibret, P. Danhier, B. Ucakar, S. Laurent, R. N. Muller, C. Jérôme, B. Gallez, V. Préat and F. Danhier, Dual anticancer drug/superparamagnetic iron oxide-loaded PLGA-based nanoparticles for cancer therapy and magnetic resonance imaging, *Int. J. Pharm.*, 2013, **447**, 94–101.

47 C. Schneider, *NIH Image to ImageJ: 25 Years of Image Analysis*, https://www.nature.com/articles/nmeth.2089?report=reader, accessed November 11, 2021.

48 S. Saini, D. D. Stark, P. F. Hahn, J. C. Bousquet, J. Introcasso, J. Wittenberg, T. J. Brady and J. T. Ferrucci, Ferrite particles: A superparamagnetic MR contrast agent for enhanced detection of liver carcinoma, *Radiol*, 1987, **162**, 217–222.

49 R. Verma, L. Mehan, R. Kumar, A. Kumar and A. Srivastava, Computational fluid dynamic analysis of hydrodynamic shear stress generated by different impeller combinations in stirred bioreactor, *Biochem. Eng. J.*, 2019, **151**, 107312.

50 R. Dinarvand, N. Sepehri, S. Manoochehri, H. Rouhani and F. Atyabi, Polylactide-co-glycolide nanoparticles for controlled delivery of anticancer agents, *Int. J. Nanomed.*, 2011, **6**, 877–895.

51 J. Panyam and V. Labhasetwar, Biodegradable nanoparticles for drug and gene delivery to cells and tissue, *Adv. Drug Delivery Rev.*, 2003, **55**, 329–347.

52 S. Y. Lin, K. S. Chen, H. H. Teng and M. J. Li, In vitro degradation and dissolution behaviours of microspheres prepared by three low molecular weight polyesters, *J. Microencapsulation*, 2000, **17**, 577–586.

53 B. S. Zolnik and D. J. Burgess, Evaluation of in vivo–in vitro release of dexamethasone from PLGA microspheres, *J. Controlled Release*, 2008, **127**, 137–145.

54 C. G. Oster and T. Kissel, Comparative study of DNA encapsulation into PLGA microparticles using modified double emulsion methods and spray drying techniques, *J. Microencapsulation*, 2005, **22**, 235–244.

55 J. v. Andhariya, J. Shen, Y. Wang, S. Choi and D. J. Burgess, Effect of minor manufacturing changes on stability of compositionally equivalent PLGA microspheres, *Int. J. Pharm.*, 2019, **566**, 532–540.

56 C. E. Astete and C. M. Sabliov, Synthesis and characterization of PLGA nanoparticles, *J. Biomater. Sci*, 2006, **17**, 247–289.

57 C. Gräfe, A. Weidner, M. v. d. Lühe, C. Bergemann, F. H. Schacher, J. H. Clement and S. Dutz, Intentional formation of a protein corona on nanoparticles: Serum concentration affects protein corona mass, surface charge, and nanoparticle–cell interaction, *Int. J. Biochem. Cell Biol.*, 2016, **75**, 196–202.